High Performance All-Polymer Solar Cell via Polymer Side-Chain Engineering

Yan Zhou, Tadanori Kurosawa, Wei Ma, Yikun Guo, Lei Fang, Koen Vandewal, Ying Diao, Chenggong Wang, Qifan Yan, Julia Reinspach, Jianguo Mei, Anthony Lucas Appleton, Ghada I. Koleilat, Yongli Gao, Stefan C. B. Mannsfeld, Alberto Salleo, Harald Ade, Dahui Zhao,* and Zhenan Bao**

The performance of organic solar cells has rapidly improved over the past few years.[1] Major efforts have been focused on developing a variety of donor materials to collect a broader wavelength range of the solar spectrum, to tune their energy levels, and to improve hole transport.[2–4] On the other hand, the most widely used acceptors are still those from the fullerene family, including [6,6]-phenyl-C_{61}-butyric acid methyl ester ($PC_{61}BM$), $PC_{71}BM$ and indene C_{60} bis-adduct (ICBA).[3,5] The high cost of fullerenes and their potential lack of morphological stability will potentially hinder the future commercialization of fullerene-based organic solar cells.[6] All-polymer solar cells, consisting of polymers for both the donor and acceptor, gained significantly increased interests recently, because of their ease of solution processing, potentially low cost, versatility in molecular design, and their potential for good chemical and morphological stability due to entanglement of polymers.[7,8] Unlike small molecular fullerene acceptors, polymer acceptors can benefit from the high mobility of intra-chain charge transport[9,10] and exciton generation by both donor and acceptor.[11] Moreover, all-polymer bulk heterojunction (BHJ) systems are considered less likely to have "dead island" formation and the associated charge recombination.[7]

Despite extensive efforts on all-polymer solar cells in the past decade, however, only a few systems had reported power conversion efficiencies (PCE) over 2%.[12–15] In early 2013, there have been two new reports with PCEs up to 3.3%[16] and 3.6%.[17–19] More recently, a PCE of 4.1% was reported.[19] Additionally, Polyera released an announcement of achieving a PCE as high as 6.47%, demonstrating the potential for high efficiency with all-polymer solar cells.[7]

Controlling phase separation is one of the most critical issues in all-polymer solar cells as it limits the generation of free charge carriers and subsequently the device performance.[7] Tuning processing parameters during device fabrication has been used to optimize phase separation.[20,21] However, limited success has been achieved in this regard. Recently, we introduced the use of polystyrene (PS) side-chains for conjugated polymers.[22] The solubility and processibility were improved for the resulting polymers with <10 mol% PS-containing repeating units, yet, the thin film transistor mobility and solar cell performance with fullerene acceptors were the same or better than without PS side chains.[22] In this paper, we report high performance all-polymer solar cells employing isoindigo-containing donor polymers and perylene tetracarboxlic di-imide (PTCDI)-containing acceptor polymers. Incorporation of polystyrene side chains into the donor polymer[22] is found to assist in reducing the phase separation domain length scale. A direct correlation between the short circuit current (J_{SC}) and the length scale of BHJ phase separation is observed. An average PCE of 4.2% from 20 devices with an average J_{SC} of 8.8 mA cm^{-2} are obtained. The highest PCE is 4.4%, with a J_{SC} as high as 9.0 mA cm^{-2}, and V_{OC} of 1.04 V. This result represents one of the highest performance in published literature for all-polymer solar cells.[7,16,17,19]

The chemical structures and energy diagrams of the donor and acceptor polymers employed herein are shown in **Scheme 1**. The isoindigo polymers are selected as the donor polymers because of their low bandgaps, strong absorption, good hole charge transport, deep HOMO for potentially high V_{OC} and good BHJ solar cell performance when combined with PCBM acceptors.[23–26] A swallow-tail substituted PTCDI polymer is chosen as the acceptor polymer due to its

Dr. Y. Zhou, Dr. T. Kurosawa, Dr. L. Fang, Dr. Y. Diao, Dr. J. Reinspach, Dr. J. Mei, Dr. A. L. Appleton, Dr. G. I. Koleilat, Prof. Z. Bao
Department of Chemical Engineering
Stanford University
Stanford, California 94305, USA
E-mail: zbao@stanford.edu

Y. Guo, Dr. Q. Yan, Prof. D. Zhao
College of Chemistry
Peking University
Beijing 100871, China
E-mail: dhzhao@pku.edu.cn

Dr. W. Ma, Prof. H. Ade
Department of Physics
North Carolina State University
Raleigh, NC 27695, USA
E-mail: hwade@ncsu.edu

Dr. K. Vandewal, Prof. A. Salleo
Department of Materials Science and Engineering
Stanford University
Stanford, California 94305, USA

Dr. Y. Diao, Dr. J. Reinspach, Dr. S. C. B. Mannsfeld
Stanford Synchrotron Radiation Lightsource
SLAC National Accelerator Laboratory
Menlo Park, California 94025, USA

C. Wang, Prof. Y. Gao
Department of Physics and Astronomy
University of Rochester
Rochester, NY 14627

DOI: 10.1002/adma.201306242

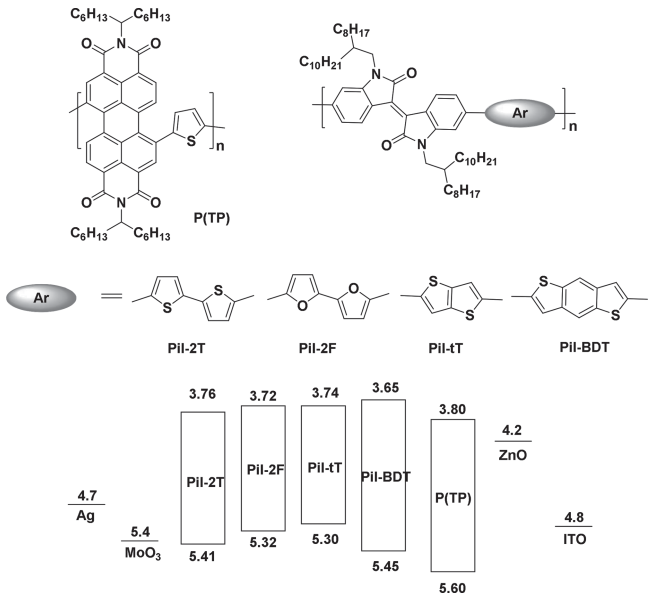

Scheme 1. Polymeric structures in all-polymer solar cell. P(TP) is the polymeric acceptor and PiI-2T, PiI-2F, PiI-tT and PiI-BDT are the polymeric donors.

good electron transporting property and good solubility.[15,27,28] All the polymer samples were synthesized from Stille coupling polymerization reactions and purified by Soxhlet followed by preparative Size Exclusion Chromatography (SEC) fractionation. The molecular weight and polydispersity index (PDI) are listed in Table S1.

As shown in **Figure 1** and Table S1, the optical band gaps of the isoindigo polymers are close to 1.6 eV while PiI-BDT gives an optical gap of 1.7 eV. The thin films of polymeric donors show two major absorption bands at around 700 nm and 650 nm, respectively. The maximum absorption peak of P(TP) is centered at 563 nm, hence complementing the absorption profile of the polymeric donors.

The energy levels of these active materials were measured by Ultraviolet Photoemission Spectroscopy (UPS) and Inverse Photoemission Spectroscopy (IPES). The LUMO levels of the donor polymers are all similar to each other at around −3.70 eV, despite the different aromatic co-monomers. The HOMO level of P(TP) was measured to be −5.72 eV by UPS, while the LUMO level was −3.80 eV by IPES. Based on the IPES measured LUMO levels, the LUMO-LUMO offset [(−3.70 eV) − (−3.80 eV)] between the donors and the acceptor is less than 0.1 eV, lower than the often mentioned empirical value of 0.3 eV needed for efficient exciton dissociation.[29] It can be seen later that despite of this very low offset, the relatively high PCE can still be achieved.

Grazing incident X-ray diffraction (GIXRD) is used to obtain the crystalline order and polymer orientation information in the polymeric donors. As shown in Figure S1, crystalline structures are found in all the donors in the thin film state while no crystalline order is observed for the acceptor polymer (data not shown). The d-spacing does not change between the neat films and blend films, for both the lamellar (100) distance and the π–π (010) distance, but the intensities of those diffraction patterns were notably lower. This data indicates that the crystallinity of the donor polymers was reduced by blending with the acceptor polymer, but the orientation of the crystalline regions remained unchanged.

Our all-polymer solar cell is constructed in an inverted BHJ structure, in which an electron transporting layer of ZnO is at the bottom and the hole transporting layer of MoO_3 is at the top. The various donor polymers with small changes in their chemical structures exhibited drastically different photovoltaic characteristics (**Table 1**). From the external quantum efficiencies (EQE) shown in **Figure 2**b, we clearly observed that features at wavelength shorter than 550 nm are overlapping with the acceptor polymer absorption region, which indicates that excitons generated on the acceptor polymer also contributed to the overall performance of the device. Normalizing the EQE over the double-pass absorption of the devices, the internal quantum efficiencies (IQEs) from 500 nm to 720 nm (Figure S2) are almost the same within each cells with different donor, suggesting that the excitons generated from donor and acceptor split with equal probability in these blends.

Interestingly, although the energy levels and absorption coefficients of the employed donor polymers are very similar to each other, the current generated from the various junctions differed drastically. In addition to the absorption spectrum, J_{SC} depends on the fraction of photogenerated excitons reaching the D-A interface, the dissociation efficiency of these excitons into free carriers and the transport efficiency of the resulting free carriers. To understand and identify the causes for the observed trend in J_{SC} we turn to analyzing the absorption, phase separation, driving force for exciton dissociation into free charge carriers and carrier mobilities.

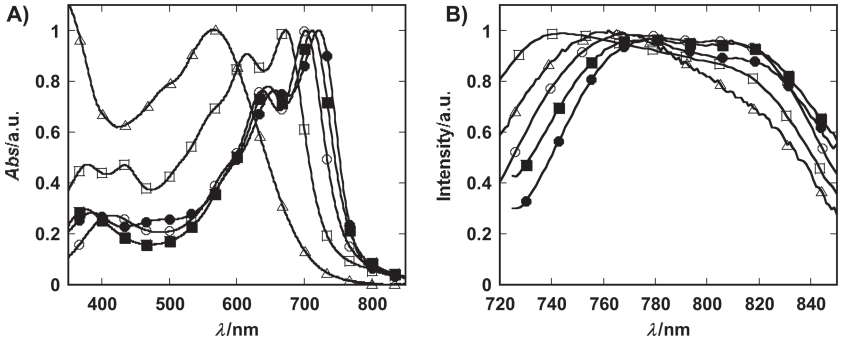

Figure 1. UV-Vis absorption spectra(A) and photo luminance spectra(B) of the donor and acceptor polymer thin films. The materials have complementary absorption features enabling the efficient capture of light across visible and part of the near infrared regions of the solar spectrum. PiI-2T (empty circle), PiI-BDT (empty square), PiI-2F (filled squares), PiI-tT (filled circle) and P(TP) (empty triangles).

In order to determine the percentage of excitons that can reach and dissociate at the donor/acceptor interface, the photoluminescence quenching efficiencies (PLQE) are measured by directly comparing the PL intensity of the polymer donor, acceptor and BHJ films under the same excitation

Adv. Mater. 2014,
DOI: 10.1002/adma.201306242

Table 1. Device characteristics of all-polymer solar cells with P(TP) as the acceptor. The Donor/Acceptor weight ratio is 1/1. The cell area is 0.040 cm^2. All cells were illuminated with AM1.5G filter at an intensity of 100 mW cm^{-2}. The cell structure is glass/ITO/ZnO/active layer/MoO_3/Ag. All the numbers are averaged from 20 devices.

Donor	PCE/%	J_{SC}/mA cm^{-2}	V_{OC}/V	FF	R_s/Ω cm^{-2}
PiI-2T	3.48 ± 0.13	6.91 ± 0.30	1.01 ± 0.01	0.50 ± 0.01	11
PiI-2T-PS5	4.21 ± 0.10	8.77 ± 0.29	1.04 ± 0.01	0.46 ± 0.01	8
PiI-BDT	3.12 ± 0.09	6.54 ± 0.14	1.07 ± 0.01	0.45 ± 0.01	30
PiI-2F	2.71 ± 0.07	5.59 ± 0.02	0.96 ± 0.00	0.51 ± 0.01	17
PiI-tT	1.67 ± 0.08	4.10 ± 0.10	0.97 ± 0.01	0.42 ± 0.01	49
PiI-tT-PS5	2.75 ± 0.06	5.92 ± 0.25	0.99 ± 0.01	0.45 ± 0.01	8

wavelength, geometry and equipment parameters. The trend in PL quenching efficiency correlates well with the observed trend in J_{SC} (shown in Figure 2c).

A poor PL quenching might be due to either large domains or energy level mismatch, which inhibits charge transfer. Resonant Soft X-ray Scattering (RSoXS) is used to obtain the phase separation characteristics of the polymer blends. This technique is essential in this case because the contrast of the scattering signal of hard X-ray is too weak from the all-polymer blends.[30–33] A resonant photon energy of 283 eV is used to enhance the contrast of the polymer:polymer blends. To confirm the RSoXS scattering is originating from the polymer:polymer phase separation, a non-resonant energy 270 eV that is less sensitive to polymer:polymer contrast but more sensitive to mass-thickness variations is also utilized. The stronger and more pronounced scattering peak at 283 eV indicates that the RSoXS measures polymer:polymer phase separation at that energy (Figure S8). The scattering profiles at 283 eV are displayed in Figure 2d and represent the distribution function of spatial frequency, $s = q/2\pi$, of the samples. The median of the distribution s_{median} corresponds to the characteristic median length scale, ξ, of the corresponding phase distribution in real space with $\xi = 1/s_{median}$. The ξ is 260 nm for PiI-tT/P(TP), 100 nm for PiI-2F/P(TP), 50 nm for PiI-BDT/P(TP) and 54 nm for PiI-2T/P(TP), respectively. The trend in the characteristic median length scale correlates well with the PL quenching efficiency as well as the J_{SC}, i.e. a smaller domain size was found to give a higher J_{SC} and a higher PLQE.

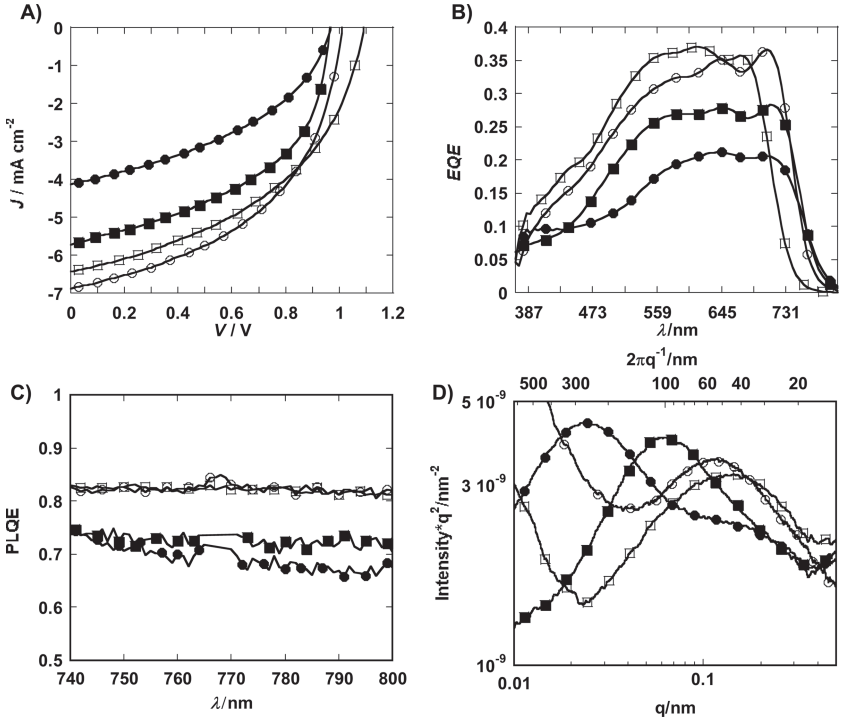

Figure 2. Solar cell behavior of the all-polymer BHJs. A) current-voltage (*J–V*) curves. B) EQE spectra of devices with different polymer donors. C) Photoluminescence quenching efficiency (PLQE) of BHJ films at different wavelengths. D) RSoXS profiles of different blend films. PiI-2T (empty circle), PiI-BDT (empty square), PiI-2F (filled squares), PiI-tT (filled circle) and P(TP) (triangle).

The dissociation of excitons into free charge carriers involves electron transfer that forms the charge transfer (CT) state, in which the electron resides on the acceptor molecule while the hole remains on the donor molecule. When such a CT state is lower in energy than the neat donor or acceptor exciton, it is characterized by weak absorption and emission at energies below the optical gap of the neat materials. Sensitive EQE measurements in the sub-gap region of most studied organic solar cell BHJs therefore reveal CT absorption.[34] The driving force for charge transfer, defined by the difference between the lowest optical gaps of the neat material and the CT state optical gap, can be deduced from such measurements.[34,35]

For our all-polymer BHJs, highly sensitive EQE measurements did not reveal any distinct sub-gap CT absorption band (Figure S3a-d). On the other hand, when using regioregular poly(3-hexylthiophene) (P3HT) with a shallower LUMO as the donor material blended with P(TP), a CT band in the P3HT gap region was clearly visible (See Figure S3e). This indicates that the absence of a sub-gap CT band for the isoindigo polymers under investigation here is due to their deeper LUMO level as compared to P3HT. The smaller LUMO-LUMO offset between the donor and acceptor resulted in a lower

driving force for charge transfer and subsequently CT state formation.

Similarly, the electroluminescence spectra of the blends showed only emission spectra resembling that of the neat donor polymer, with no CT band observed (Figure S3). This again confirms that the CT state in these BHJs is very high in energy, close to the energy of the excitons in the neat material. In some cases (Figure S3a) the peak positions of EL and EQE of the blends were even blue shifted as compared to the pure material. This is probably due to a decrease in aggregation of the isoindigo polymer upon blending.

The employments of both EQE and EL spectra enable the accurate determination of the optical gaps of the neat donor polymers and blends. Based on the above values, the V_{OC} of the devices correlates well with the deduced optical gap of the blend ($V_{OC} = E_g - 0.6$ V). The absence of a subgap CT absorption or emission band correlation indicate that for all the blends studied in this work, the energy loss due to electron transfer is minimized, hence maximizing the V_{OC}. It is remarkable that despite the lack of a large driving force for electron transfer, a decent charge generation (6.5 mA cm^{-2}) is still possible in these materials. Similar observations have been reported before for other isoindigo polymer:PCBM BHJs.[36,37]

The mobilities measured from space-charge limited current (SCLC) are listed in Table S3. The hole mobilities in the blend films are all around 2×10^{-4} cm^2 V^{-1} s^{-1}, while the acceptor polymer P(TP) has a lower electron mobility of 2×10^{-5} cm^2 V^{-1} s^{-1}. The hole mobilities of the donors do not correlate well to the J_{SC}, indicating that the charge transport efficiency of the devices may be limited by the low electron mobility of the acceptor polymer. The absorption (A(E)) of the blend films was in the similar range, indicating that the differences of the J_{SC} were not originated from the absorption difference either (Figure S4).

The above characterizations suggest that phase separation domain size is the most significant factor that gives rise to the dramatically different device performance. Therefore, we proceed to modify the best polymer donor polymer by attaching a small percentage of PS side chains to demonstrate a new route to control phase separation behavior in all-polymer blends (Scheme S1).[22] With such polymer side-chain modification, we expected to reduce the domain size in the blend film by reducing the strong tendency for self-aggregation in the D-A donor polymer. In fact, the average PCE of the PiI-2T-PS5/P(TP), in which 5 mol% of the repeating units in PiI-2T are attached with PS side chains, reached 4.2%, with a J_{SC} as high as 8.8 mA cm^{-2}, and a V_{OC} of 1.04 V. The highest measured PCE was up to 4.4%, and J_{SC} was as high as 9.0 mA cm^{-2}. From RSoXS data in **Figure 3**c, the median domain size (30 nm) of these devices was indeed 45% smaller than that formed by the PiI-2T/P(TP) blend (54 nm).

To test the applicability of the PS-side-chain modification approach to other donor polymers, the same modification on the worst performing donor polymer PiI-tT is performed. After being modified by 5 mol% of PS side-chain, the PCE of PiI-tT-PS5/P(TP) increased to 2.75% from 1.67%, with a J_{SC} as high as 5.92 mA cm^{-2}, and a V_{OC} of 0.99 V(Shown in Figure S5). The phase separation length scale of the blend film, measured by RSoXS, was reduced from 260 nm to 50 nm by attaching 5% PS side chains in the donor polymer. In this case (Figure S5), the PLQE increased from 66% to 76% after the attachment of PS side-chain, confirming again a reduction of the domain length scale and a more efficient exciton dissociation.

Different device fabrication conditions are utilized to optimize the device performance. Annealing temperatures from 80 to 140 °C are applied to the active films prior to the thermal evaporation of the electrodes. Similar *J*–*V* curves are obtained indicating that phase separations of the polymers blends were stable under different thermal annealing conditions (Figure S7). The PCEs of devices are not very sensitive to the donor/acceptor blend ratios from 5/4 to 4/5. These robust fabrication features are highly desirable for future large scale production.

In conclusion, a side-chain engineering approach using polystyrene enables manipulation of phase separation domain size and enhances all-polymer solar cell performance to reach PCE as high as 4.4%. A J_{SC} as high as 9.0 mA cm^{-2} is obtained with a donor-acceptor pair despite of a low LUMO-LUMO energy offset of less than 0.1 eV. The phase separation domain length scale correlates well with the J_{SC} and is found to be highly sensitive to the aromatic co-monomer molecular structures used

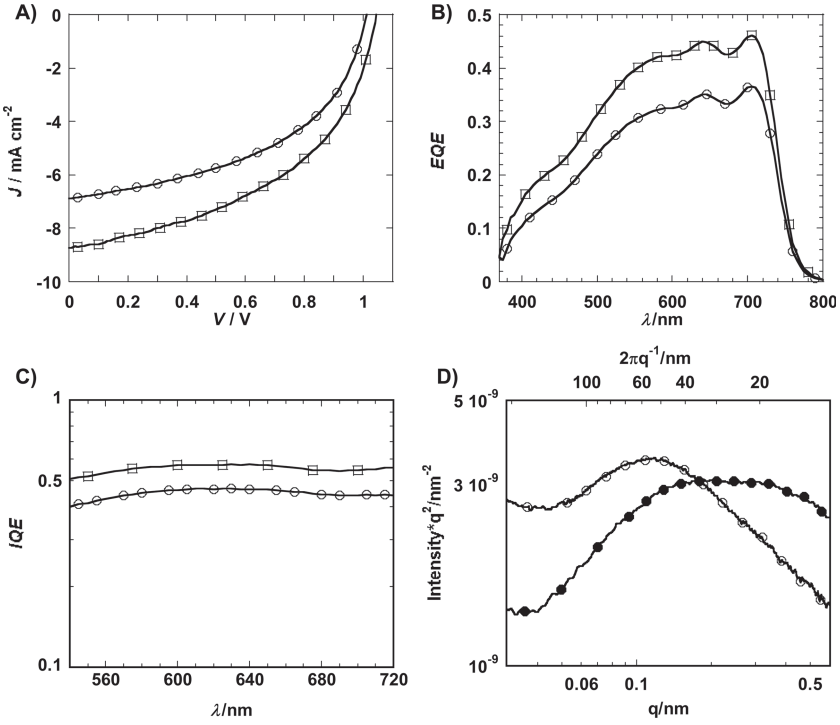

Figure 3. *J*–*V* curves(A), EQE spectra(B), IQE spectra(C) and RSoXS scatering features of solar cell made by PiI-2T/P(TP) (circles) and PiI-2T-PS5/P(TP) (squares).

Adv. Mater. **2014**,
DOI: 10.1002/adma.201306242

in the crystalline donor polymers. With the PS polymer side-chain engineering, the phase separation domain length scale decreased by more than 45%. The PCE and J_{SC} of the devices increased accordingly by more than 20%. This work demonstrates that a better understanding of tuning polymer phase separation domain size provides an important path towards high performance all-polymer solar cells. The use of polymer side-chain engineering provides an effective molecular engineering approach that may be combined with additional processing parameter control to further elevate the performance of all-polymer solar cells.

Experimental Section

General Method: All the polymers were synthesized according to previously reported procedures.[15, 22, 24] All the polymers were purified via preparation SEC at room temperature with chloroform as solvent. The molecular weight and PDI of all polymers were measured by high temperature GPC with 1,2,4-trichlorobenzene as the solvent and polystyrenes as the calibration standards at 160 °C.

2D-GIXD images were collected in reflection mode with a planar area detector in a He atmosphere at beamline 11–3 of the Stanford Synchrotron Radiation Lightsource. The sample–detector distance was nominally set to 400 mm, and the incidence angle was 0.12°; the X-ray wavelength was 0.9758 Å. Slits were set to 150 and 50 μm in the horizontal and vertical directions, respectively.

R-SoXS measurements were performed at beamline 11.0.1.2 at the Advanced Light Source.[38] The sample films used for R-SoXS were spin-cast on sodium polysulfonate covered glass as substrate. To carry out R-SoXS experiment in transmission, the film is floated off in deionized water and picked up with a 1.5 mm by 1.5 mm silicon nitride window. The film is then dried in air before being transferred into the vacuum chamber for R-SoXS.

Photoemission spectroscopy of occupied and unoccupied states of the system was performed using a VG ESCA Lab system equipped with both UPS and IPES. The spectrometer chamber of the UHV system had a base pressure of 8×10^{-11} Torr. Occupied states (or valence band) spectra were obtained by UPS using the unfiltered He I line (21.2 eV) of a discharge lamp with the samples biased at −5.0 V to avoid the influence of the detector work function and to observe the true low-energy secondary cutoff. The typical instrumental resolution for UPS measurements ranges from 0.03 to 0.1 eV with photon energy dispersion of less than 20 meV.

Unoccupied states (or conduction bands) were measured by IPES using a custom-made spectrometer composed of a commercial Kimball Physics ELG-2 electron gun and a bandpass photon detector prepared according to an existing design. IPES was done in the isochromat mode using a photon detector centered at a fixed energy of 9.8 eV. The combined resolution (electron + photon) of the IPES spectrometer was determined to be 0.6 eV from the width of the Fermi edge measured on a clean polycrystalline Au film. The UPS and IPES energy scales were aligned by measuring the position of the Fermi level on a freshly evaporated Au film. The position of the vacuum level, E_{vac}, was measured for each surface using the onset of the secondary cutoff in the UPS spectra. All the measurements were done at room temperature.

Absorption spectra were recorded on a Cary 6000i Spectrometer. The PL spectra were obtained from a Horiba Jobin-Yvon FluoroMax-4 Luminescence Spectrometer.

Solar Cell Fabrication and Testing: Glass substrates coated with patterned indium-doped tin oxide (ITO) with a sheet resistance of 13 Ω /□ was purchased from Xin Yan Technology Lt. Before device fabrication, the ITO/glass substrates were subjected to a series of wet-cleaning processes in an ultrasonic bath sequentially in acetone, detergent, deionized water and isopropanol. After dried in the vacuum oven at 80 °C for 10 mins and followed by a 20-min UV-Ozone treatment, ZnO sol-gel was spun-coated onto the ITO surface at a speed of 4000 rpm for 18 s.[39] The ZnO was baked at 200 °C for 0.5 h in air to formed a 30 nm thick film. The polymers were dissolved into 1,2-dichlorobenzene with stirring over night at 100 °C. The concentration was 10 mg/mL for PiI-2T, PiI-2T-PS5 and PiI-2F, and 20 mg/mL for PiI-BDT, PiI-tT and P(TP), respectively. The blend solutions were freshly made prior spin-coating and kept at 50 °C. All the active layers were spun-coated at 700 rpm for 25 s in the glove box. The wet films were put into a covered Petri dish and allowed to dry at room temperature overnight. The dried films were subsequently annealed in the glove box at 100 °C for 5 mins before they were transferred to a vacuum evaporator for electrode deposition. The thickness of the active layer was 100 nm for PiI-2T/P(TP) and PiI-2F/P(TP), 93 nm for PiI-2T-PS5/P(TP), 120 nm for PiI-BDT/P(TP), 180 nm for PiI-tT/P(TP), measured by a Dektak surface profiler. A MoO_3 layer (15 nm) followed by a Ag layer (70 nm) were thermally deposited at a pressure of 6×10^{-6} Torr. The device active area is 4.0 mm^2. All the devices were tested inside a nitrogen glove box with less than 40 ppm O_2 and 4 ppm H_2O. The PCE was tested under AM 1.5G illumination with an intensity of 100 mW cm^{-2} (Newport Solar Simulator 94021A) calibrated by a Newport certified silicon photo diode covered with KG5 filter with active area as 0.0663 cm^2, comparable to our device area of 0.04 cm^2.[40] The *J–V* curves were recorded with a Keithley 2400 semiconductor analyzer. The IPCE and double-pass absorption were measurements under monochromic illumination and the calibration of the incident light intensity was performed with a calibrated silicon photodiode. The double-pass absorptions measurements were carried out in an integrating sphere and the parasitic absorptions of the electrode materials calculated by transfer matrix were deducted. For the sensitive EQE measurements, the current from the devices was measured as a function of photon energy using a lock-in amplifier (Stanford Instruments SR 830). For IQE calculation, the parasitic absorptions were calculated by transfer matrix optical modelling.[41]

Electroluminescence spectra were measured using a spectrograph (Acton Research SpectraPro 500i) equipped with a silicon CCD (charge-coupled device) array detector (Hamamatsu). The spectra were corrected for the instrument response.

Supporting Information

Supporting Information is available from the Wiley Online Library or from the author.

Acknowledgements

Acknowledge support from the Office of Naval Research (N00014-14-1-0142), KAUST Center for Advanced Molecular Photovoltaics at Stanford and the Stanford Global Climate and Energy Program, NSF DMR-1303742 and the National Natural Science Foundation of China (Projects 21174004 and 21222403). Soft X-ray characterization and analysis by NCSU supported by the U.S. Department of Energy, Office of Science, Basic Energy Science, Division of Materials Science and Engineering under Contract DE-FG02–98ER45737. Soft X-ray data was acquired at beamlines 11.0.1.2 at the Advanced Light Source, which is supported by the Director, Office of Science, Office of Basic Energy Sciences, of the U.S. Department of Energy under Contract No. DE-AC02–05CH11231. We thank Professor Michael D. McGehee, Dr. George F. Burkhard and Dr. Eric T. Hoke for their help in discussion of the recombination mechanism.

Received: December 22, 2013
Revised: February 18, 2014
Published online:

[1] G. Li, R. Zhu, Y. Yang, *Nat. Photon.* **2012**, *6*, 153.
[2] J. Nelson, *Mater. Today* **2011**, *14*, 462.
[3] Y. Lin, Y. Li, X. Zhan, *Chem. Soc. Rev.* **2012**, *41*, 4245.
[4] J. Chen, Y. Cao, *Acc. Chem. Res.* **2009**, *42*, 1709.
[5] P. Sonar, J. P. Fong Lim, K. L. Chan, *Energy Environ. Sci.* **2011**, *4*, 1558.
[6] B. A. Collins, J. R. Tumbleston, H. Ade, *J. Phys. Chem. Lett.* **2011**, *2*, 3135.
[7] A. Facchetti, *Mater. Today* **2013**, *16*, 123.
[8] M. Jørgensen, K. Norrman, S. A. Gevorgyan, T. Tromholt, B. Andreasen, F. C. Krebs, *Adv. Mater.* **2012**, *24*, 580.
[9] P. Prins, F. C. Grozema, J. M. Schins, S. Patil, U. Scherf, L. D. A. Siebbeles, *Phys. Rev. Lett.* **2006**, *96*, 146601.
[10] L. Fang, P. Liu, B. R. Sveinbjornsson, S. Atahan-Evrenk, K. Vandewal, S. Osuna, G. Jimenez-Oses, S. Shrestha, G. Giri, P. Wei, A. Salleo, A. Aspuru-Guzik, R. H. Grubbs, K. N. Houk, Z. Bao, *J. Mater. Chem. C* **2013**, *1*, 5747.
[11] Y. Liu, T. T. Larsen-Olsen, X. Zhao, B. Andreasen, R. R. Sondergaard, M. Helgesen, K. Norrman, M. Jorgensen, F. C. Krebs, X. Zhan, *Sol. Energ. Mat. Sol. Cells* **2013**, *112*, 157.
[12] D. Mori, H. Benten, H. Ohkita, S. Ito, K. Miyake, *ACS Appl. Mater. Interfaces* **2012**, *4*, 3325.
[13] T. W. Holcombe, J. E. Norton, J. Rivnay, C. H. Woo, L. Goris, C. Piliego, G. Griffini, A. Sellinger, J.-L. Brédas, A. Salleo, J. M. J. Fréchet, *J. Am. Chem. Soc.* **2011**, *133*, 12106.
[14] E. Zhou, J. Cong, Q. Wei, K. Tajima, C. Yang, K. Hashimoto, *Angew. Chem. Int. Ed.* **2011**, *50*, 2799.
[15] Y. Zhou, Q. Yan, Y.-Q. Zheng, J.-Y. Wang, D. Zhao, J. Pei, *J. Mater. Chem. A* **2013**, *1*, 6609.
[16] T. Earmme, Y.-J. Hwang, N. M. Murari, S. Subramaniyan, S. A. Jenekhe, *J. Am. Chem. Soc.* **2013**, *135*, 14960.
[17] E. Zhou, J. Cong, K. Hashimoto, K. Tajima, *Adv. Mater.* **2013**, *25*, 6991
[18] P. Cheng, L. Ye, X. Zhao, J. Hou, Y. Li, X. Zhan, *Energy & Environmental Science* **2014**, 10.1039/c3ee43041c.
[19] D. Mori, H. Benten, I. Okada, H. Ohkita, S. Ito, *Adv. Energ. Mater.* **2013**, 10.1002/aenm.201301006.
[20] D. Mori, H. Benten, J. Kosaka, H. Ohkita, S. Ito, K. Miyake, *ACS Appl. Mater. Inter.* **2011**, *3*, 2924.
[21] M. Schubert, D. Dolfen, J. Frisch, S. Roland, R. Steyrleuthner, B. Stiller, Z. Chen, U. Scherf, N. Koch, A. Facchetti, D. Neher, *Adv. Energ. Mater.* **2012**, *2*, 369.
[22] L. Fang, Y. Zhou, Y.-X. Yao, Y. Diao, W.-Y. Lee, A. L. Appleton, R. Allen, J. Reinspach, S. C. B. Mannsfeld, Z. Bao, *Chem. Mater.* **2013**, *25*, 4874.
[23] R. Stalder, J. Mei, K. R. Graham, L. A. Estrada, J. R. Reynolds, *Chem. Mater.* **2014**, *26*, 664.
[24] T. Lei, Y. Cao, X. Zhou, Y. Peng, J. Bian, J. Pei, *Chem. Mater.* **2012**, *24*, 1762.
[25] E. Wang, Z. Ma, Z. Zhang, K. Vandewal, P. Henriksson, O. Inganäs, F. Zhang, M. R. Andersson, *J. Am. Chem. Soc.* **2011**, *133*, 14244.
[26] R. Stalder, J. Mei, J. R. Reynolds, *Macromolecules* **2010**, *43*, 8348.
[27] Q. Yan, Y. Zhou, Y.-Q. Zheng, J. Pei, D. Zhao, *Chem. Sci.* **2013**, *4*, 4389.
[28] X. Zhang, Z. Lu, L. Ye, C. Zhan, J. Hou, S. Zhang, B. Jiang, Y. Zhao, J. Huang, Y. Liu, Q. Shi, J. Yao, *Adv. Mater.* **2013**, *25*, 5791.
[29] D. Veldman, S. C. J. Meskers, R. A. J. Janssen, *Adv. Funct. Mater.* **2009**, *19*, 1939.
[30] H. Yan, B. A. Collins, E. Gann, C. Wang, H. Ade, C. R. McNeill, *ACS nano* **2011**, *6*, 677.
[31] S. Swaraj, C. Wang, H. Yan, B. Watts, J. Lüning, C. R. McNeill, H. Ade, *Nano lett.* **2010**, *10*, 2863.
[32] C. Wang, D. H. Lee, A. Hexemer, M. I. Kim, W. Zhao, H. Hasegawa, H. Ade, T. P. Russell, *Nano lett.* **2011**, *11*, 3906.
[33] L. Ye, S. Zhang, W. Ma, B. Fan, X. Guo, Y. Huang, H. Ade, J. Hou, *Adv. Mater.* **2012**, *24*, 6335.
[34] J. Lee, K. Vandewal, S. R. Yost, M. E. Bahlke, L. Goris, M. A. Baldo, J. V. Manca, T. Van Voorhis, *J. Am. Chem. Soc.* **2010**, *132*, 11878.
[35] J.-L. Brédas, J. E. Norton, J. Cornil, V. Coropceanu, *Acc. chem. res.* **2009**, *42*, 1691.
[36] K. Vandewal, Z. Ma, J. Bergqvist, Z. Tang, E. Wang, P. Henriksson, K. Tvingstedt, M. R. Andersson, F. Zhang, O. Inganäs, *Adv. Funct. Mater.* **2012**, *22*, 3480.
[37] Z. Ma, W. Sun, S. Himmelberger, K. Vandewal, Z. Tang, J. Bergqvist, A. Salleo, J. W. Andreasen, O. Inganas, M. R. Andersson, C. Muller, F. Zhang, E. Wang, *Energ. Environ. Sci.* **2014**, 10.1039/c3ee42989j.
[38] E. Gann, A. T. Young, B. A. Collins, H. Yan, J. Nasiatka, H. A. Padmore, H. Ade, A. Hexemer, C. Wang, *Rev. Sci. Instru.* **2012**, *83*, 045110.
[39] Y. Sun, J. H. Seo, C. J. Takacs, J. Seifter, A. J. Heeger, *Adv. Mater.* **2011**, *23*, 1679.
[40] H. J. Snaith, *Energ. Environ. Sci.* **2012**, *5*, 6513.
[41] G. F. Burkhard, E. T. Hoke, M. D. McGehee, *Adv. Mater.* **2010**, *22*, 3293.

Adv. Mater. **2014**,
DOI: 10.1002/adma.201306242